PHILOSOPHICAL TRANSACTIONS B

royalsocietypublishing.org/rstb



Research

**Cite this article:** Girkin N *et al.* 2026 Environmental controls over greenhouse gas dynamics of tropical peatlands of the Central Congo Basin. *Phil. Trans. R. Soc. B* **381**: 20240482.
https://doi.org/10.1098/rstb.2024.0482

Received: 11 May 2025
Accepted: 12 August 2025

One contribution of 17 to a discussion meeting issue 'African tropical peatlands: function, value and vulnerability'.

**Subject Areas:**
environmental science, ecosystem, ecology

**Keywords:**
methane, nitrous oxide, carbon dioxide, tropical peatlands, Cuvette Centrale, FTIR, Rock-Eval pyrolysis, climate change, hydrology

**Author for correspondence:**
Nicholas Girkin
e-mail: Nicholas.Girkin@nottingham.ac.uk

Supplementary material is available online at https://doi.org/10.6084/m9.figshare.c.8566722.

THE ROYAL SOCIETY PUBLISHING

# Environmental controls over greenhouse gas dynamics of tropical peatlands of the Central Congo Basin

Nicholas Girkin[1], Alice Johnston[2], Hayley Curran[1], Sofie Sjögersten[1], A. Jonay Jovani-Sancho[1,3], Yannick Enock Bocko[4], Pierre Bola[5], Arnoud Boom[6], Hannah Cooper[1], Bart Crezee[7], Dafydd Egryn Crabtree[3], Greta Dargie[7], Ovide Emba Botuli[8], Joseph Kanyama[9], Ian Lawson[10], Yeto Emmanuel Wenina Mampouya[11], Mackline Mbemba[11], Vicky Moss-Hayes[12], Guy Rodrigue Mouanda Niamba[13], Susan E. Page[6], Kirby Robinson[6], Christopher H. Vane[12], Corneille E. N. Ewango[14], Suspense Ifo[15] and Simon L. Lewis[7]

[1]School of Biosciences, University of Nottingham, Nottingham, UK
[2]Faculty of Engineering and Applied Sciences, Cranfield University, Cranfield, UK
[3]Centre for Ecology and Hydrology Bangor Site, Bangor, UK
[4]Faculty of Science and Technology, [5]École Normale Supérieure d'Agronomie et de Foresterie and [6]École Normale Supérieure, Marien Ngouabi University, Brazzaville, Congo
[7]Institut Supérieur Pédagogique Mbandaka, Mbandaka, Congo
[8]School of Geography, Geology and the Environment, University of Leicester, Leicester, UK
[9]School of Geography, University of Leeds, Leeds, UK
[10]Faculté des sciences, Département de biologie, Université de Kinshasa, Kinshasa, Congo
[11]Department of Ecology and Forest Management, University of Kisangani, Kisangani, Congo
[12]Department of Geography and Sustainable Development, University of St Andrews, St Andrews, UK
[13]Organic Geochemistry Facility, British Geological Survey, Nottingham, UK
[14]Wildlife Conservation Society, Epena, Congo
[15]University of Kisangani, Kisangani, Congo

NG, 0000-0001-7562-5775; YEB, 0000-0002-3358-6218; BC, 0000-0002-1459-6402; DEC, 0000-0001-7502-8823; GD, 0000-0002-1871-6360; SLL, 0000-0002-8066-6851

The central Congo Basin hosts the world's largest tropical peatland complex, storing 29.0 Pg of carbon, the equivalent to three years of global $CO_2$ emissions. These peatlands are significant natural sources of greenhouse gases (GHGs), including $CO_2$, $CH_4$ and $N_2O$, but the environmental controls on their emissions remain poorly understood. To address this, we collected surface peat samples from six regional landscapes, spanning palm- and hardwood-dominated sites, and incubated them under three hydrological regimes: flooded aerobic, flooded anoxic and mesic (aerobic and no surface water). This allowed us to quantify how hydrology and peat chemistry (carbon, nutrients and organic chemistry) influence GHG dynamics. We observed strong differences in GHG production between vegetation types, and high sensitivity to hydrological change. Using random forest models, we assessed 27 potential drivers of GHG fluxes, identifying distinct controls across GHGs and hydrological regimes. Incubation of deeper peat samples (up to 1.5 m) highlighted that surface layers dominate peat GHG production. Taken together, our findings demonstrate that hydrology, vegetation, nutrients and peat organic chemistry shape regional GHG emissions, driving substantial spatial variability. Changes to peatland hydrology, for

example from land use or climate change, could significantly shift GHG balances, with important implications for global climate feedbacks. A French translation of this abstract is available in the supplementary material.

This article is part of the discussion meeting issue 'African tropical peatlands: function, value and vulnerability'.

## 1. Introduction

Tropical peatlands are a globally important carbon sink, but also an important natural source of rising atmospheric concentrations of greenhouse gases (GHGs), including methane ($CH_4$), nitrous oxide ($N_2O$) and carbon dioxide ($CO_2$). The central Congo Basin is home to the world's largest tropical peatland, covering approximately 145 000 $km^2$ and storing approximately 29 pg of carbon, equivalent to three years of global anthropogenic $CO_2$ emissions [1], but the scale of GHG emissions, and their underlying drivers, remain poorly understood [2].

Peatlands in the central Congo Basin are typically characterized by two dominant vegetation types: hardwood-dominated swamp forest and palm-dominated swamp forest, usually dominated by *Raphia laurentii* [2–4]. Previous work indicates that while inundation is key for determining emissions, vegetation also has a critical role in moderating the balance of consumptive and productive processes [5]. Hydrological regime determines the balance between anoxic conditions (under which $CH_4$ production dominates) and aerobic conditions (under which $CO_2$ production dominates, driven by soil respiration and $CH_4$ oxidation), with changes in temperature determining rates of decomposition [5,6]. $N_2O$ is predominantly produced through canonical nitrification and denitrification, a series of microbially driven pathways requiring aerobic conditions for nitrification and anoxic conditions for denitrification [7,8]. Plant inputs determine initial peat chemical properties and peat microbial community composition and function [5,9]. Tropical peats with contrasting botanical origins (for example, peats derived from hardwood-dominated versus palm-dominated vegetation) have distinct organic matter profiles which can, in turn, impact decomposition rates and the net balance of GHG emissions [10–12]. For example, Hoyos-Santillan *et al.* [12] demonstrated through an *ex situ* laboratory incubation of peat cores from a neotropical peatland in Panama that high $CO_2$ and $CH_4$ production in surface peats under anoxic conditions was likely driven by concentrations of lignin, fatty acids and polysaccharides, as key substrates for respiration and methanogenesis [12], but did not identify any significant differences in emissions between dominant vegetation types. By contrast, Sjögersten *et al.* [6] identified significant differences in potential production from surface peats from peats derived from contrasting botanical origins at neighbouring sites, with higher emissions from peat derived from palm (*Raphia taedigera*) compared to hardwood-dominated (*Campnosperma panamensis*) and mixed species Panamanian peat swamp forest [6].

Beyond the importance of vegetation in determining organic matter properties, plant vascular tissues can act as an important pathway for the transport of GHGs from the peat to the atmosphere [13]. Roots can further moderate emissions through inputs of oxygen, which can mitigate peat surface methane emissions [5], and root exudates can be an important substrate for GHG production and impact peat chemistry at local scales around the rooting zone [14,15]. However, the intricacies of these plant regulatory processes increase the heterogeneity of in-field emissions and thus complicate efforts to assess the balance of production and consumption processes and quantify the importance of other critical drivers of GHG dynamics [2,5,16]. Quantifying the controls over emissions is essential, given the scale of potential GHG emissions from tropical peatlands, the sensitivity of GHG production and consumption pathways to climate warming and changes in hydrological regime driven by altered flooding regimes, precipitation or drainage [6,17]. Understanding the balance of such processes for peatlands in the central Congo Basin is vital, given its global importance as a carbon sink, storing the equivalent of three years of global $CO_2$ emissions [3].

In this study, we aimed to assess the key drivers of potential GHG production/consumption for peatlands in the central Congo Basin and quantify the extent to which processes differ between dominant peat-forming vegetation types (palm versus hardwoods) using an *ex situ* laboratory incubation. We incubated surface peat samples from six peatland sites spanning the Republic of Congo and Democratic Republic of Congo, featuring a mix of hardwood- versus palm-derived peats, measuring a range of chemical properties previously identified as potential drivers of fluxes—including peat organic chemistry, total carbon and nitrogen and a range of macro- and micronutrients. We concurrently measured changes in potential emissions using peat samples incubated down core to a depth of 170 cm from two contrasting sites dominated by hardwood trees and palms in the Republic of Congo, to test how production and consumption processes varied with depth. We sought to address the following questions: (i) how do contrasting hydrological regimes impact GHG fluxes, (ii) how do peat biogeochemical properties vary between peats from contrasting sites and botanical origins (hardwood versus palms), and (iii) to what extent do key drivers differ between contrasting hydrological regimes and peats derived from contrasting botanical origins?

## 2. Methods

### (a) Study sites

The peatlands of the central Congo Basin are characterized by hardwood and palm peat swamp forests. Rainfall is approximately 1760 mm $yr^{-1}$, with two distinct wet seasons each year, peaking in April and May, and in October and November. The intervening dry periods are relatively short and rarely intense. Mean annual temperature is 25.6°C with limited intra-annual variation [18,19].

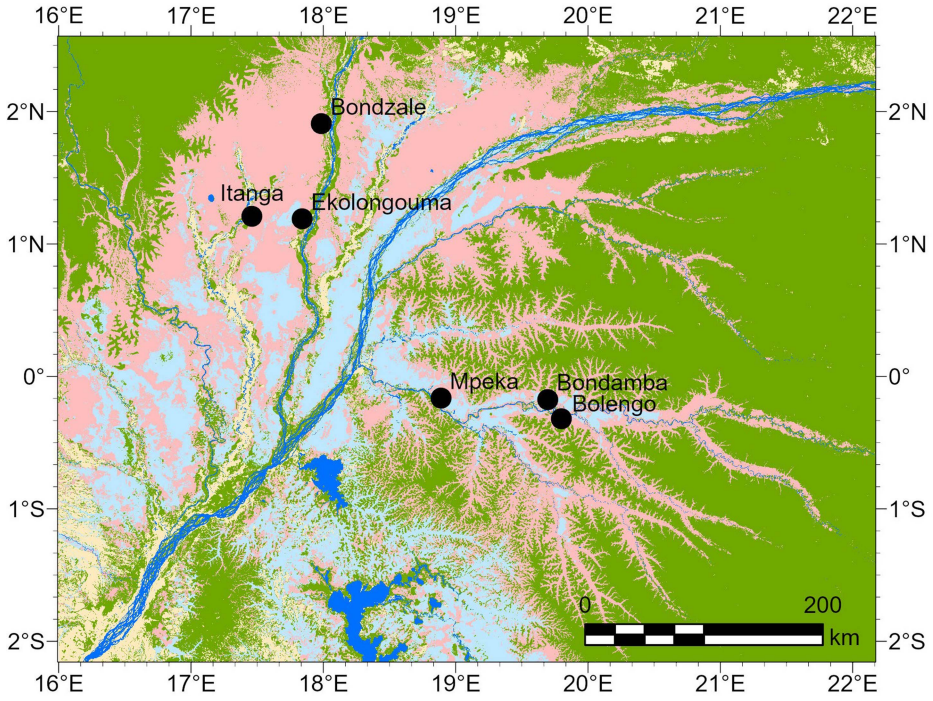


**Figure 1.** Peatland study sites in the central Congo Basin spanning the Republic of Congo and Democratic Republic of Congo [3], including water bodies (dark blue), savannah (yellow), non-peat forming forest (terra firme and seasonally inundated forest, green), palm-dominated peat swamp forest (pink) and hardwood-dominated peat swamp forest (light blue).

Peat samples were collected from sites located along transects spanning six peatland sites (informally named after the nearest villages) in the Republic of Congo (Ekolongouma, Itanga and Bondzale, all interfluvial sites) in January–March 2019, and Democratic Republic of Congo (Bolengo, Bondamba and Mpeka, all river-influenced sites) in June–July 2019 (figure 1). The 5 km Bondzale transect, 11 km Ekolongouma transect and 5 km Itanga transect are all in the Likouala province of the Republic of Congo. Sites featured a range of palm- and hardwood-dominated peat swamp forest, with the former featuring *Raphia laurentii*, and the latter a range of hardwood species including *Carapa procera*. Water levels at the time of sampling were approximately 20–30 cm below the peat surface. The 10 km Mpkea, 7 km Bondamba and 8 km Bolengo transects were located on the Busira River in the Democratic Republic of Congo. Palm-dominated peat swamp included both *Raphia sese* and *Raphia laurentii*, while hardwood-dominated peatland areas included *Cryptosepalum congolanum*, *Pseudagrostistachys ugandensis*, *Carapa procera*, *Guibourtia demeusei* and *Prioria oxyphylla*. Water levels at the time of sampling were approximately 20 cm below the peat surface.

To analyse trends in GHG emissions down peat profiles, and the extent to which they differed between peat derived from contrasting vegetation types, four replicate cores were collected from palm-dominated and hardwood-dominated peatland sites, approximately 1 km apart, located near the village of Ekolongouma, in the Republic of Congo. Peat cores were extracted using a side-filling Russian Peat Corer (Van Walt, UK) with a 50 cm long sampling chamber. Peat depth was determined at every site by recording the distance from the peat surface to the underlying mineral layer. Following extraction, peat samples were divided into 10 cm segments and then bagged and sealed to prevent moisture loss [9].

## (b) Greenhouse gas production assays

Potential GHG production from surface peats was assessed using a series of laboratory incubations, with samples subjected to three moisture treatments: flooded anoxic, flooded aerobic and mesic conditions. The anaerobic treatment models long-term raised water tables. The flooded aerobic treatment models oxygenated high water table conditions (e.g. following rainfall). The mesic treatment models low surface moisture during periods of low rainfall when water tables drop, but also provides an approximate indication of responses to drainage.

For the incubation, 120 ml serum bottles (Kinesis, St Neots, UK) were filled with 10 g of field-moist peat from each sample collected from the peat surface (0–20 cm). For the anoxic treatment, 10 ml of deionized water was added to the peat and gently swirled for two minutes to mix. The resulting peat/water mixture was bubbled vigorously with $N_2$ to create oxygen-free conditions and to fill the headspace with $N_2$ [5]. The bottles were then capped using black butyl stoppers and crimped, and the bottles were placed in their incubator for one month to allow the microbial communities to acclimate. A 5 ml gas sample was taken from the bottle and analysed for $CO_2$, $CH_4$ and $N_2O$ using gas chromatography (see below for details) to assess anaerobic gas production. This sampling was repeated twice, one month apart.

For the flooded aerobic (oxygenated) treatment, the headspace was aerated and then placed on an orbital shaker for approximately 2 minutes to encourage oxygen mixing, with the process repeated daily over 5 days to stimulate heterotrophic activity during initial acclimation. Bottles were then left in incubators at 25°C for one month for acclimation before aerobic GHG production rates were assessed. This was done by first bubbling with air of known concentration, five replicate samples of which were collected for gas chromatograph (GC) analysis. After flushing, the headspace bottles were capped using butyl stoppers. The bottles were immediately returned to their incubators for 1 hour after which a 5 ml gas sample was taken from each bottle for the determination of GHG concentrations. Gas fluxes were calculated using the concentration difference between the initial headspace concentrations and those after 1 hour's incubation [6].

The mesic moisture treatment involved incubation of the uncapped bottles at 25°C to allow moisture to evaporate from the bottles, reflecting natural evaporation conditions during low rainfall periods. The evaporation rate differed among samples, and, rather than letting the peat dry for a set time, we regularly checked the peat moisture status visually; conditions were considered mesic when there was no pooled water visible, but the peat was still moist. Bottles were then covered in parafilm and placed back in their respective temperature incubators for one month to equilibrate. GHG production rates were assessed by bubbling with air, as described above [6].

Down-core patterns in GHG production were assessed in a second, separate experiment. Fresh peat (10 g) from 10 cm thick samples across a range of depths was weighed into 48 replicate 120 ml serum bottles. As previous studies have demonstrated that peat GHG production rises closer to the peat surface, the majority of samples used were from between 0 and 100 cm, with only two samples from below this depth (100–110 cm and 170–180 cm). Peat samples in this experiment were incubated under flooded anoxic, flooded aerobic and mesic conditions created as described above.

All GHG samples in both studies were analysed by gas chromatography (GC 2014, Shimadzu, Milton Keynes, UK) using a 1 ml sampling loop and a molecular sieve column (12 m, 0.53 mm internal diameter). $CO_2$ concentrations were determined by thermal conductivity, $CH_4$ by flame ionization and $N_2O$ concentration using an electron capture device. GHG fluxes were calculated using the ideal gas law for sampling points which met the assumption of linear (or near linear) gas accumulation during the closure period [14,15].

## (c) Peat physico-chemical analyses

Homogenized peat sub-samples ($n = 4$) were used to characterize physico-chemical properties to 20 cm depth. Gravimetric moisture content (SM) was determined from the mass lost from 10 g of wet peat, oven dried at 105°C for 24 h. Peat organic matter content (LOI) was determined as the mass lost after ignition for 7 h at 550°C in a muffle furnace. Bulk density was measured by collecting intact 10 × 10 × 25 cm sections from the peat surface, oven drying at 105°C for 24 h and weighing. Total peat carbon (C) and total nitrogen (N) content were determined from 0.2 g of dry, homogenized peat combusted using a total element analyser (Flash EA 1112, CE Instruments, Wigan, UK) [10]. pH and electrical conductivity were determined using a glass electrode and a portable conductivity meter (Hanna Instruments), respectively, in a 1: 2.5 ratio of fresh peat to deionized water.

## (d) Rock-Eval ® pyrolysis

Down-core peat sub-samples were analysed using a Rock-Eval 6 analyser, following established methods for peat soils [5,9,20–22]. Freeze-dried powdered peat samples (60 mg) were heated at 300°C for 3 min before an increase in temperature to 650°C at a rate of 25°C per minute in an inert $N_2$ atmosphere. Residual carbon was oxidized from 300 to 850°C at a rate of 20°C per minute. The release of hydrocarbons during the two-stage pyrolysis process was detected by a flame ionization detector, with an infrared cell detecting the release of CO and $CO_2$ during the thermal cracking of the organic matter. Rock-Eval analysis generated a range of standard parameters including S1 (a measure of free hydrocarbons released on heating to 300°C), S2 (hydrocarbons released on the thermal cracking of organic matter for temperatures up to 650°C), S3CO and S3$CO_2$ (the CO and $CO_2$ yielded from the breakdown of kerogen), Tpk2 (the temperature associated with the highest yield of bound hydrocarbons) and total organic carbon ($TOC_{RE}$). Here, we focused on two new indices, I and R, describing the preservation of thermally labile and highly thermostable organic matter, respectively, which have been used extensively in the characterization of tropical peat organic chemistry [5,9,20,21,23,24]. Both indices were calculated using the approach proposed by Sebag *et al.* [25] using the integrated areas under the S2 curve between given temperature nodes. Areas were calculated as 200–340°C (A1), 340–400°C (A2), 400–460°C (A3) and greater than 460°C (A4). The I-index (previously associated with more thermally labile organic matter) was calculated as log((A1 + A2)/A3), and the R-index (associated typically with more thermally stable and recalcitrant organic matter) was calculated as (A3 + A4)/100.

## (e) ATR-FTIR

Attenuated Total Reflectance Fourier transform infrared (ATR-FTIR) absorption spectra for peat surface samples were obtained with a Bruker Tensor 27 FTIR equipped with a nitrogen purge gas generator and a mercury–cadmium–telluride detector. A total of 128 scans were performed on each oven-dried, ball-milled sample, and background spectra were run initially and after every eight samples. Absorptions in the spectral range spanned from 550 to 4000 $cm^{-1}$ at a resolution of 1 $cm^{-1}$. All spectra were standardized, smoothed and baseline corrected (SpectraGryph v. 1.2) before statistical analysis in order to allow direct comparison [26]. We used 1630 : 1030 as the ratio of C = C stretch aromatic from lignin bonds and C-O stretch from carbohydrate bonds, reflecting the lignin: carbohydrate ratio [27].

### (f) Data processing and statistical analysis

Outliers (measurements over two standard deviations above or below the mean) were removed from the gas chromatography data, including 35 values for $CO_2$, 33 values for $CH_4$ and 20 values for $N_2O$. Overall, our assessment of potential production/consumption included 915 measurements for $CO_2$, 917 for $CH_4$ and 930 for $N_2O$. To meet statistical test assumptions, downcore GHG production/consumption data were natural log-transformed. Data was analysed using R (v. 4.5.0; [28]).

We used linear mixed effects models with restricted maximum likelihood estimation (REML) to evaluate significant differences in GHGs and all measured environmental variables across sites and vegetation types. Fixed effects included vegetation type and site, while site was also treated as a random effect where appropriate to account for nested sampling structure. Separate models were also constructed to evaluate vertical trends in GHG concentrations and peat chemistry with depth. All models were run independently for each response variable to capture specific patterns and associations.

To investigate associations between GHG concentrations ($CO_2$, $CH_4$ and $N_2O$) and peat biogeochemical properties across distinct hydrological regimes, we computed Pearson correlation coefficients within each treatment. A total of 27 variables were tested, including all GHG concentrations, distance from river (DfR_km), pH, electrical conductivity (EC), gravimetric soil moisture (SM), total carbon (TC), total nitrogen (TN), sodium (Na), magnesium (Mg), phosphorus (P), sulfur (S), potassium (K), calcium (Ca), aluminium (Al), manganese (Mn), iron (Fe), cobalt (Co), nickel (Ni), copper (Cu), zinc (Zn), molybdenum (Mo), cadmium (Cd), lead (Pb) and the FTIR-derived lignin: carbohydrate ratio (1630 : 1030 $cm^{-1}$). Data were grouped by hydrological regime, and for each group, a pairwise Pearson correlation matrix was computed between $CO_2$, $CH_4$ or $N_2O$ and other variables. The strongest nine correlation pairs (based on the absolute correlation coefficient) were retained for visualization with heatmaps to visualize correlation strengths. Hierarchical clustering, based on Euclidean distance and complete linkage, was applied to the correlation matrices for each treatment to reorder variables and highlight clusters of strongly associated parameters.

We further investigated differences in surface peat chemistry across vegetation types and sites by applying non-metric multidimensional scaling (NMDS) using Bray–Curtis dissimilarities with the metaMDS() function from the vegan package [29]. To inform the selection of environmental variables included in ordination, we used results from the correlation matrix analysis, retaining only those variables most strongly correlated with GHG concentrations ($CO_2$, $CH_4$ and $N_2O$). Highly collinear variables were removed to reduce redundancy, resulting in a final selection of 13 variables (Mg, SM, Fe, P, Cu, Ni, Co, K, pH, TC, S, Zn and Pb). Ordination results were visualized with ellipses grouped by vegetation type (palm- versus hardwood-dominated). To identify which variables were significantly associated with variation in peat chemistry, we fitted environmental vectors using 999 permutations, with $p < 0.05$ considered significant.

To explore nonlinear and interactive controls on GHG fluxes, we used Random Forest (RF) regression models. Separate models were trained for standardized $CO_2$, $CH_4$ and $N_2O$ fluxes in each of the three hydrological regimes using five-fold cross-validation. A total of 24 environmental predictors were tested, including vegetation, landscape setting (interfluvial for Bondzale, Itanga and Ekolongouma sites, versus river-influenced for Bondamba, Bolengo and Mpeka sites), peat physico-chemical properties and elemental concentrations. Predictor importance was evaluated using permutation-based variable importance, and partial dependence plots were used to visualize individual predictor effects.

## 3. Results

### (a) Spatial patterns in potential greenhouse gas production and peat chemistry

$CO_2$ production responded significantly to changing moisture levels across treatments (figure 2; $p < 0.001$), with the highest production under mesic conditions (4164.5 ng $CO_2$ $g^{-1}$ $h^{-1}$), followed by flooded aerobic (3628.2 ng $CO_2$ $g^{-1}$ $h^{-1}$) and flooded anoxic conditions (941.9 ng $CO_2$ $g^{-1}$ $h^{-1}$). Production was greatest from palm-dominated peat (3269.1 versus 2421.0 ng $CO_2$ $g^{-1}$ $h^{-1}$; $p < 0.001$), and varied significantly with distance from rivers (lowest at 1 km, increasing at 2 km and subsequently gradually declining; $p < 0.001$) and between sites ($p < 0.001$).

$CH_4$ production/consumption potential also responded significantly to changing moisture levels across treatments (figure 3; $p < 0.001$), with the highest production under flooded anoxic conditions (3.08 ng $CH_4$ $g^{-1}$ $h^{-1}$), followed by flooded aerobic conditions (2.35 ng $CH_4$ $g^{-1}$ $h^{-1}$) and mesic conditions (0.89 ng $CH_4$ $g^{-1}$ $h^{-1}$). Production/consumption potential differed significantly with distance ($p = 0.002$), in the interactions between treatment and distance ($p < 0.001$) and treatment, vegetation type and distance ($p = 0.009$). There was no significant difference in $CH_4$ production/consumption potential between vegetation types ($p = 0.549$) or between sites ($p = 0.539$); neither the interaction between treatment and vegetation ($p = 0.677$) nor the interaction between vegetation and distance ($p = 0.509$) was significant.

$N_2O$ production/consumption potential varied significantly between treatment and distance ($p = 0.001$), and vegetation type and distance ($p = 0.04$), but in contrast to $CO_2$ and $CH_4$, did not vary significantly between treatments (figure 4; $p = 0.064$). For both vegetation types, production was greatest from flooded aerobic conditions (2.1 and 2.4 ng $N_2O$ $g^{-1}$ $h^{-1}$ for hardwood- and palm-dominated peats, respectively). Production was greatest for the flooded aerobic treatment at 8 km (5.5 ng $N_2O$ $g^{-1}$ $h^{-1}$), for the flooded anoxic treatment at 1 km (3.4 ng $N_2O$ $g^{-1}$ $h^{-1}$) and for mesic conditions at 5 km (2.8 ng $N_2O$ $g^{-1}$ $h^{-1}$).

Peat chemical properties exhibited a broad range of differences between sites, dominant vegetation types and the interaction between them (supplementary material, table S1). Gravimetric moisture content (SM), redox potential (measured *in situ*), Mn and 1630 : 1030 (lignin-to-carbohydrate ratio) varied significantly between palm (85.8%, 500 mV, 40.0 µg $g^{-1}$, 0.56) and hardwood (82.3%, 370 mV, 10.7 µg $g^{-1}$, 0.66; $p < 0.001$). pH, gravimetric moisture, organic matter content, total carbon,

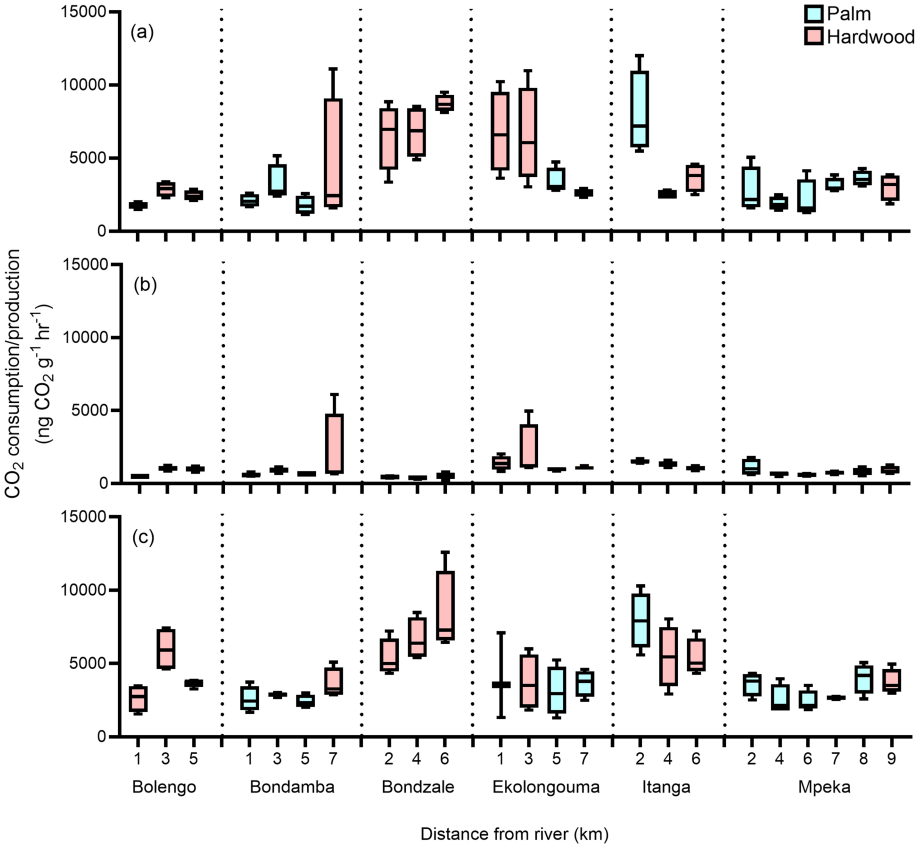


**Figure 2.** $CO_2$ production potential from six sites 1–9 km from the nearest river for (a) flooded aerobic; (b) flooded anoxic; and (c) mesic treatments ($n = 4$). Means ± 1 s.e.m.

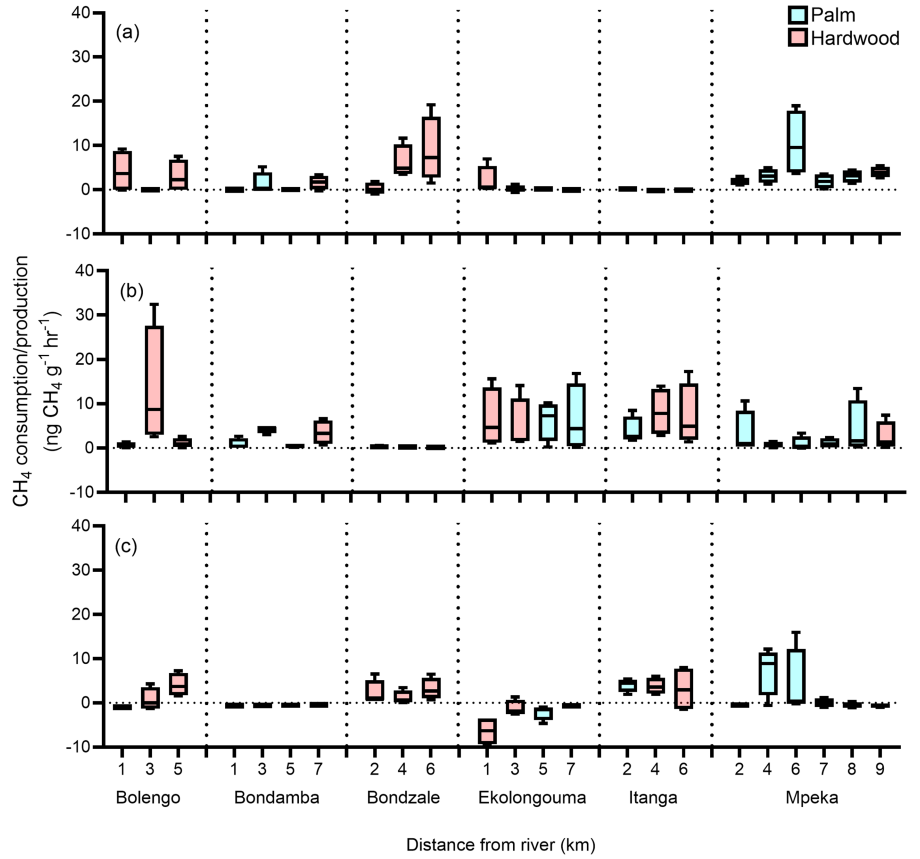


**Figure 3.** $CH_4$ production/consumption potential from six sites 1–9 km from the nearest river for (a) flooded aerobic; (b) flooded anoxic; and (c) mesic treatments ($n = 4$). Means ± 1 s.e.m.

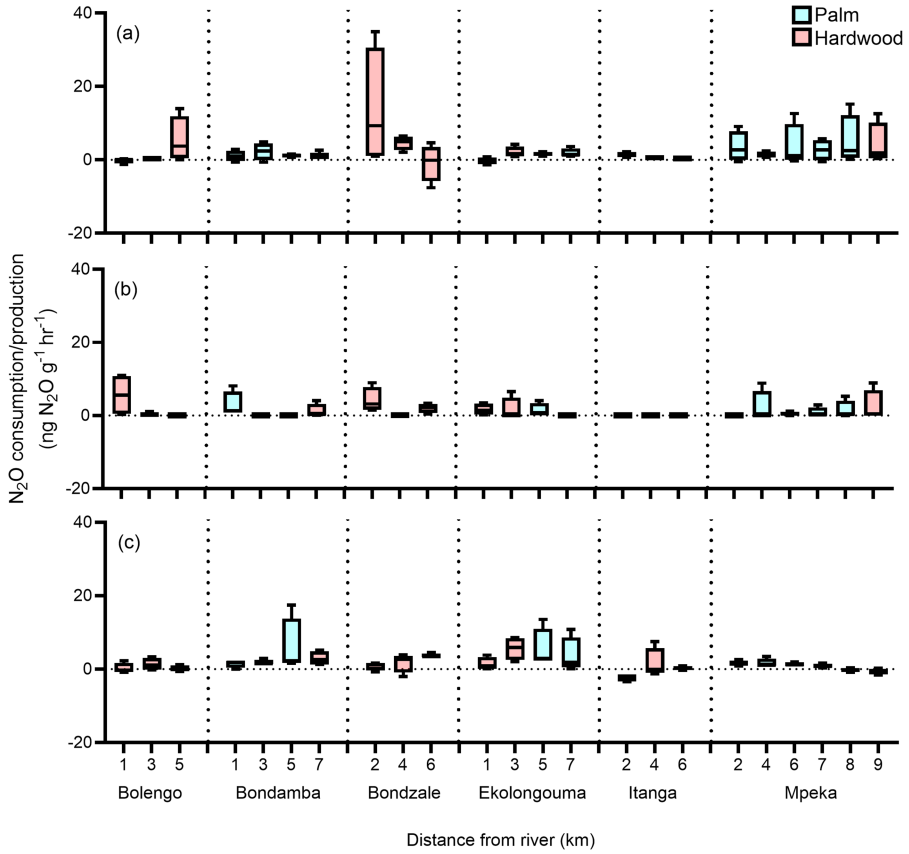


**Figure 4.** $N_2O$ production/consumption potential from six sites 1–9 km from the nearest river for (a) flooded aerobic; (b) flooded anoxic; (c) mesic treatments ($n = 4$). Means ± 1 s.e.m.

total nitrogen, redox potential, electrical conductivity, Cu, Fe, Mn, P, S and lignin : carbohydrate (1630:1030 derived from FTIR) all varied significantly between sites ($p < 0.001$). pH, organic matter content, redox potential and lignin : carbohydrate varied significantly with distance. Soils were consistently acidic, ranging from 3.46 at 4 km to 3.88 at 9 km. Organic matter content was consistently high (> 90%), greatest at 9 km (96.4%) and lowest at 4 km (90.3%). Redox potential was greatest at 8 km (608 mV) and lowest at 2 km (386 mV). Cu was greatest at 4 km (6.0 µg $g^{-1}$), Mn was greatest at 3 km (84.8 µg $g^{-1}$) and P was greatest at 2 km (810.0 µg $g^{-1}$). Lignin : carbohydrate was greatest at 7 km (0.73), and was lowest at 8 km (0.52). In general, there was no consistent trend with distance for all variables. SM, organic matter content, redox potential, Cu, Mn and P varied significantly in the interaction between vegetation and distance ($p < 0.001$), while organic matter, electrical conductivity, Cu, Fe, K, Mn and P varied significantly in the interaction between site and distance ($p < 0.001$).

## (b) Greenhouse gas fluxes and peat properties with depth

$CO_2$ and $CH_4$ fluxes varied significantly with depth ($p = 0.006$, figure 5a,b and $p < 0.001$, figure 5c,d, respectively), with potential production greatest in the upper 0–40 cm, and subsequently declining with depth. $N_2O$ fluxes did not vary significantly with depth ($p = 0.06$; figure 5e,f). There was no significant difference in fluxes of any GHG between vegetation types ($p = 0.114$, $p = 0.589$ and $p = 0.788$ for $CO_2$, $CH_4$ and $N_2O$ production/consumption potential, respectively), but there were significant differences between treatments for all GHGs ($p < 0.001$). There were significant interactions for $CH_4$ between depth and site ($p = 0.036$), and depth and treatment ($p = 0.007$), but no significant interactions were identified for $N_2O$ and $CO_2$ ($p > 0.05$).

Organic matter content decreased significantly with depth ($p < 0.001$), varied significantly between vegetation types, and showed a significant interaction between depth and vegetation type ($p < 0.001$; Figure 6a). The I-index (describing the proportion of labile carbon, derived from Rock-Eval pyrolysis), varied significantly with depth ($p < 0.001$) and vegetation ($p = 0.003$; figure 6). The I-index was greatest at the surface and rapidly declined thereafter, albeit with a small peak at 160 cm depth for cores from the palm-dominated peatland, which overall had a lower mean value (–0.05 for palm versus –0.01 for hardwood-dominated peat). By contrast, the R-index did not vary significantly between sites ($p = 0.082$), but did vary significantly with depth ($p < 0.001$; figure 6c).

## (c) Multi-variate analysis of peat chemistry

The strength and structure of correlations between GHG fluxes and peat chemistry varied substantially between hydrological treatments (figure 7). Mesic treatments show moderate positive correlations for $N_2O$, Zn, Cd and Ca, while $CH_4$ and $CO_2$ were

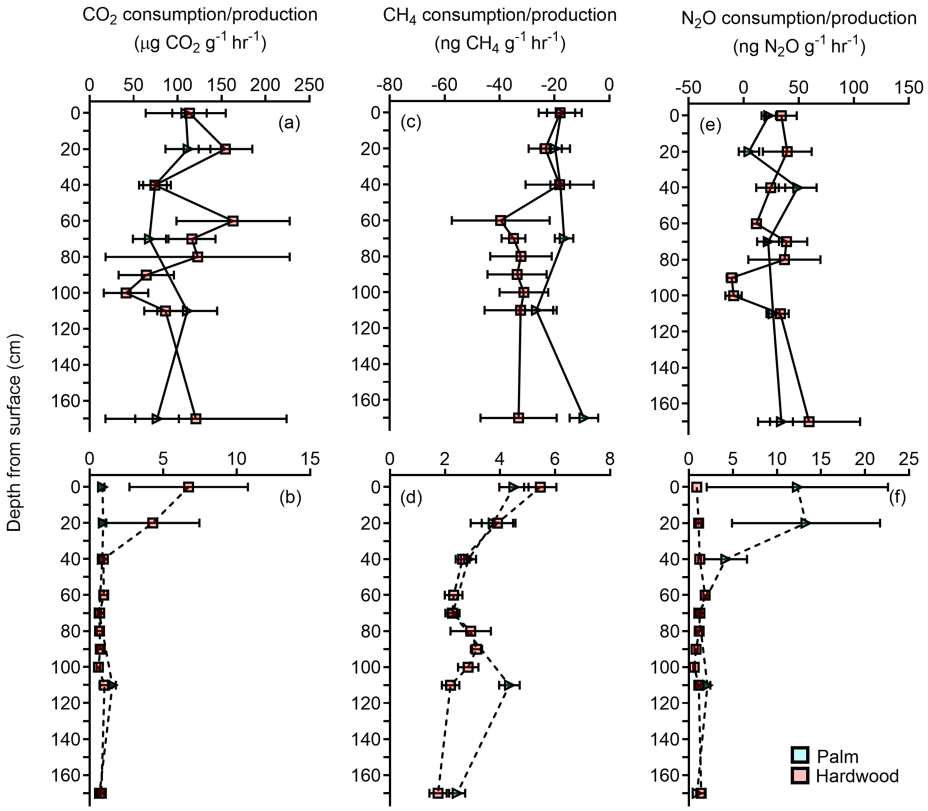


**Figure 5.** $CO_2$ fluxes from (a) aerobic and (b) anoxic; $CH_4$ fluxes from (c) aerobic and (d) anoxic; and $N_2O$ fluxes from (e) aerobic and (f) anoxic treatments between 0 and 170 cm, for peats spanning two dominant vegetation types measured at palm- and hardwood-dominated sites ($n = 4$). Note, scale bars differ on all *x*-axes. Means ± 1 s.e.m.

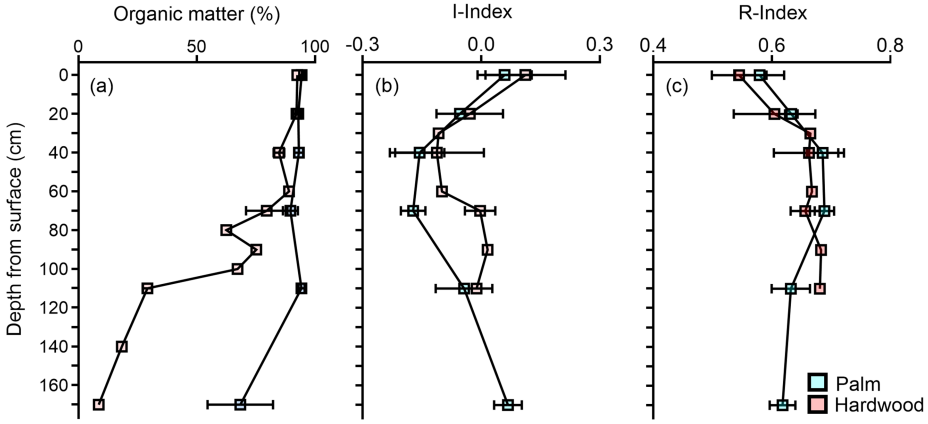


**Figure 6.** (a) Organic matter content, (b) I-index (broadly describing the labile fraction), (c) R-index (broadly describing the recalcitrant fraction) for cores ($n = 4$) from hardwood- and palm-dominated peatlands at Ekolongouma ($n = 4$). Means ± 1 s.e.m.

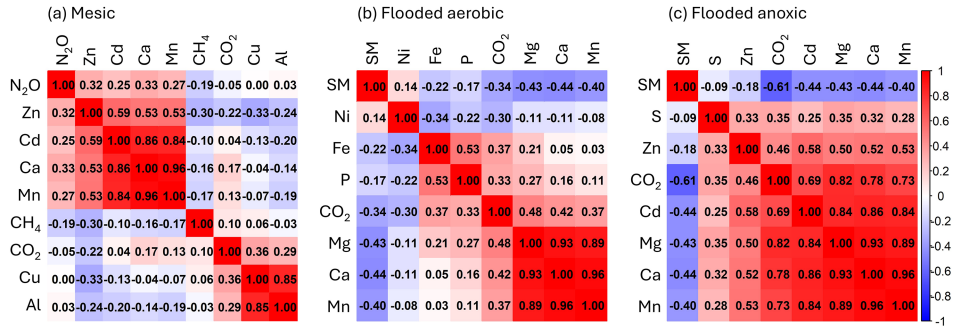


**Figure 7.** Hierarchically clustered Pearson correlation matrices for GHG fluxes and peat chemistry variables under (a) mesic, (b) flooded aerobic and (c) flooded anoxic conditions. Values represent Pearson correlation coefficients (r), with variables ordered by hierarchical clustering (complete linkage) and colour intensity indicating correlation strength (red, positive; blue, negative). Each matrix shows Pearson correlation coefficients among the subset of variables involved in the nine strongest correlations with either $CO_2$, $CH_4$ or $N_2O$ (excluding GHG–GHG correlations).

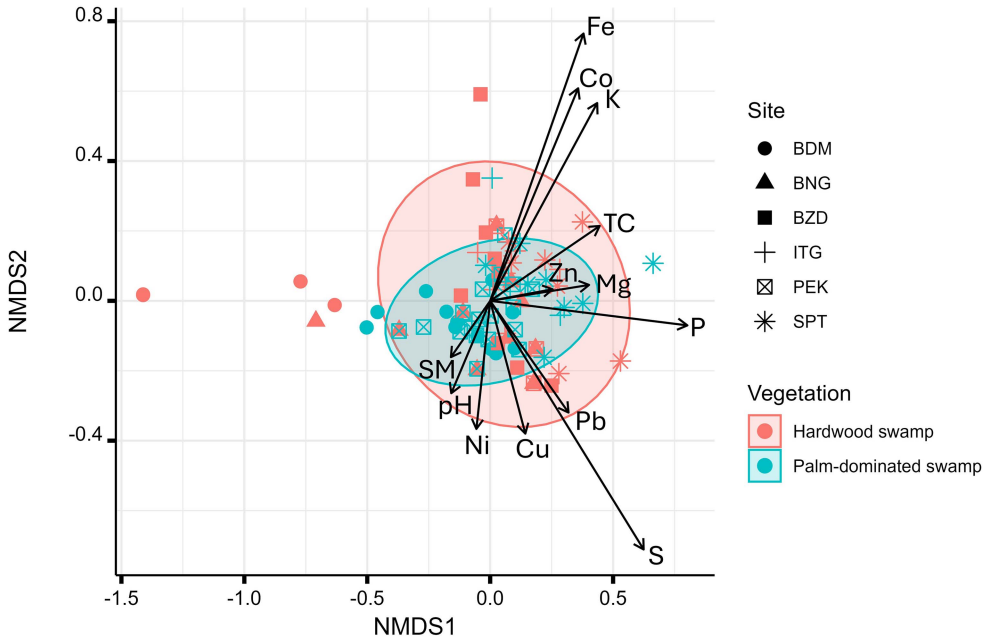


**Figure 8.** NMDS ordination of surface peat chemistry in palm- and hardwood-dominated peatlands. Points represent individual surface peat samples, with ellipses indicating 95% confidence intervals around group centroids by vegetation type. Arrows represent environmental variables significantly associated with variation in peat chemistry ($p < 0.05$) based on permutation tests ($n = 999$). Vector direction indicates the gradient, and arrow length reflects the strength of correlation (see supplementary material, table S2 for vector $R^2$ and $p$ values).

weakly correlated with these and other metals (figure 7a). In the flooded aerobic regime, $CO_2$ exhibited negative correlations with Ni, SM and Fe, while Mg and Ca showed stronger positive associations (figure 7b). By contrast, the flooded anoxic regime displayed consistently strong positive correlations between $CO_2$ and multiple elements (Cd, Mg, Ca and Mn), along with a clear clustering of these variables with high inter-correlation (figure 7c). SM was negatively correlated with most variables in the flooded anoxic regime, suggesting contrasting environmental controls under anoxic conditions. Figure 7 highlights distinct shifts in the relationship between GHG concentrations and peat chemistry shift under hydrological regimes, with the strongest associations under anoxic flooded conditions.

NMDS of peat surface chemistry revealed clear compositional differences between palm- and hardwood-dominated swamp forests (figure 8). The two-dimensional NMDS solution had a stress value of less than 0.15 (stress = 0.66), indicating a good fit between the ordination distances and the underlying Bray–Curtis dissimilarities. Environmental vector fitting identified multiple peat chemistry variables that were significantly related to the ordination pattern ($p \leq 0.003$ for all variables and 999 permutations; see supplementary material, table S2). Variables accounting for the highest levels of variation in ordination space included S ($R^2 = 0.896$), Fe ($R^2 = 0.729$), P ($R^2 = 0.649$) and K ($R^2 = 0.510$). Additional significant but weaker drivers included TC, Cu, Mg and pH ($R^2 = 0.09$–$0.24$; supplementary material, table S2). The vectors in figure 8 illustrate how variation in redox-sensitive and nutrient-associated elements structures peat chemical composition between vegetation types, with ellipses indicating clear clustering and thus distinct biogeochemical profiles between palm- and hardwood-dominated peatlands.

RF models were used to identify key predictors of GHG concentrations across hydrological regimes, owing to the robustness of these models to non-linearity, multi-collinearity and high-dimensional data. Models revealed distinct environmental controls on GHG concentrations, with the relative importance of variables linked to nutrient availability, metal concentrations and substrate quality varying substantially across hydrological regimes (table 1, figure 9).

Model performance varied across GHGs and regimes, with predictive performance for $CO_2$ highest under flooded aerobic conditions ($R^2 = 0.38$), and $CH_4$ and $N_2O$ models performing best in the mesic regime ($R^2 = 0.28$ and 0.19, respectively). By contrast, models under flooded anoxic conditions explained less variance ($R^2 = 0.12$–$0.17$, table 1). Variable importance rankings indicated that factors related to substrate quality (e.g. total carbon and lignin : carbohydrate ratio), redox-sensitive metals (e.g. Fe, Mn and Zn) and landscape context (e.g. distance from river and vegetation type) were dominant predictors, but their influence varied by GHG and hydrological regime (figure 9).

## 4. Discussion

### (a) Peat biogeochemical properties

We found substantial differences in a range of biogeochemical properties for surface peats derived from hardwood- and palm-dominated peat swamp forest (supplementary material, table S1; figure 7). Previous work has demonstrated similar variability in chemical properties between peats derived from contrasting dominant vegetation types. For example, Girkin *et al.* [10]

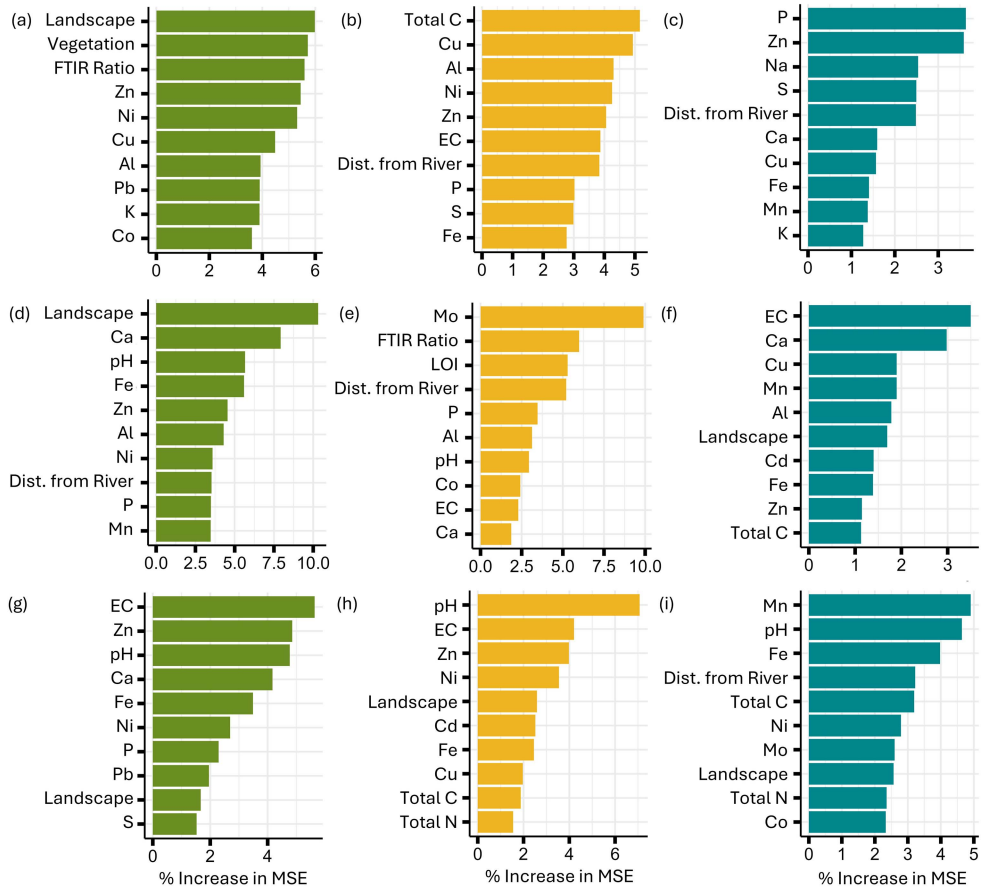


**Figure 9.** Variable importance plots for RF models predicting (a,d,g) $CO_2$, (b,e,h) $CH_4$ and (c,f,i) $N_2O$ production/consumption potentials across (a–c) mesic, (d-f) flooded aerobic and (g–i) flooded anoxic hydrological regimes. Importance is expressed as the percentage increase in mean squared error (% increase in MSE) when each variable is randomly permuted, with higher values indicating greater influence on model accuracy (see table 1 for model performance statistics).

**Table 1.** RF model performance metrics for each GHG and hydrological regime. Metrics reported include root mean square error (RMSE), coefficient of determination ($R^2$) and mean absolute error (MAE).

| hydrological regime | GHG | RMSE | $R^2$ | MAE |
|---|---|---|---|---|
| mesic | $CO_2$ | 0.482 | 0.281 | 0.370 |
| | $CH_4$ | 1.382 | 0.283 | 0.934 |
| | $N_2O$ | 1.526 | 0.187 | 0.995 |
| flooded aerobic | $CO_2$ | 0.640 | 0.380 | 0.486 |
| | $CH_4$ | 1.500 | 0.159 | 1.065 |
| | $N_2O$ | 2.750 | 0.050 | 1.042 |
| flooded anoxic | $CO_2$ | 0.153 | 0.171 | 0.102 |
| | $CH_4$ | 2.249 | 0.118 | 1.651 |
| | $N_2O$ | 1.278 | 0.099 | 0.919 |

demonstrated contrasting patterns of spatial variability in pH and organic matter content and quality from hardwood- and palm-derived peats in Central America (Panama), with similar patterns reported elsewhere, including Peru [30], and in response to changes in land use in Southeast Asian peatlands [21].

Contrasts in peat organic matter properties are likely to reflect the interaction of a range of biotic and abiotic environmental variables. We found differences in organic matter properties with depth (figure 6c) between hardwood- and palm-derived peat samples, with deeper peats tending to be more depleted in labile carbohydrates and featuring a larger thermostable pool of carbon

[9,20], with the caveat that modern vegetation does not necessarily match peat-forming vegetation down core. Differences in chemical properties of leaf, stem and shoot litter from hardwood and palm species have previously been explained by contrasting litter decomposition rates at the peat surface and within depth profiles [12]. In surface peats, palm litter has previously been reported to decompose more quickly than hardwood litter, possibly because of higher nitrogen content. However, in waterlogged soils, the inhibition of aerobic ligninolytic microorganisms reduces the rate of decomposition [31]. Palm litter has previously been reported to have higher content of p-coumaryl alcohol than hardwood litter in leaf, root and shoot material. By contrast, hardwood litter has higher content of coniferyl and sinapyl alcohols [32]. Such differences in litter chemistry have been linked to differences in physiology between monocotyledonous (palms) versus dicotyledonous (hardwood) species. Monocotyledonous palms develop hydroxyl phenol-guaicyl-syringyl lignin, containing higher amounts of lignin moieties related to p-coumaryl and sinapyl [33]. By contrast, dicotyledonous trees develop hardwood lignin, which contains higher amounts of coniferyl alcohol [33]. The rapid decomposition of litter at the surface in tropical wetlands can also be enhanced by insects such as termites that preferentially decompose cellulose, increasing the proportion of lignin content, which would be observed as a rise in Rock-Eval-based R index [34].

## (b) Rates of greenhouse gas production

The scale of potential $CO_2$ emissions from Central African peat in this study was broadly comparable to the scale of previously reported laboratory-measured production for both Panamanian and Southeast Asian peatlands [5,6,35], with production generally greater nearer to the peat surface [36]. High $CO_2$ emissions from both flooded aerobic and mesic treatments imply that oxygen inputs are strong drivers of decomposition processes, even under flooded conditions [6]. Within peat, $CO_2$ can be produced directly by microbial decomposition, and through the oxidation of $CH_4$ [5], which can occur under both mesic and flooded aerobic conditions, but which can be limited under flooded anoxic conditions [6].

We found higher $CO_2$ production from peat samples from the palm swamp forest than from the hardwood swamp forest, matching similar previous findings [6]. Peats derived from palms have previously been proposed to have increased availability of labile substrate for decomposition, providing additional substrate for methanogenesis [36]. Differing $CO_2$ emissions between peats derived from contrasting vegetation types (e.g. palm versus hardwood) have previously been reported in the tropics *in situ*, linked to similar contrasts in organic chemistry [5,10,37].

We found that $CH_4$ emissions varied significantly across treatments, being greatest under anoxic conditions, most likely owing to a lack of oxygen driving methanogenesis/inhibiting methanotrophy [5]. In keeping with previous *ex situ* studies (e.g. [35]), we found limited differences in $CH_4$ production between palm- and hardwood-derived peats (figures 3 and 5). However, *in situ*, differences between dominant vegetation types can be more pronounced owing to greater contrasts in substrate availability (e.g. through litter input and root turnover) [11,12] and plant root inputs of carbon and oxygen [5,38]. In keeping with previous studies [36], production was generally greater towards the peat surface (figure 5b), most likely driven by greater substrate availability (figure 6a–c).

We found no difference in $N_2O$ production between treatments or vegetation types. Nitrification, the sequential oxidation of ammonium to nitrite and nitrate, and denitrification, the reduction of nitrate to $N_2O$ and dinitrogen, are recognized as the dominant processes in wetland soil nitrogen dynamics [7,8,39,40], but there is little published data on the scale of emissions from peatlands not converted for agriculture [7]. Overall, the balance of these processes is determined by substrate supply of both nitrogen (denitrification and nitrification), carbon (denitrification), oxygen availability, moisture content and pH. Both processes can potentially occur simultaneously in different microsites (micrometres) within the peat owing to differences in oxygen availability. Nitrifiers can release $N_2O$ at low oxygen availability when the moisture content is equivalent to 60% water filled pore space [41]. Similarly, denitrifiers preferentially produce $N_2O$ under low oxygen conditions. The proportion of $N_2O$ as the end product of denitrification (as opposed to $N_2$) increases at lower pH and may thus represent the dominant gaseous nitrogen production pathway in tropical wetlands.

Results measured in laboratory incubations cannot and should not be directly translated to field equivalent fluxes or emissions owing to the additional complexities of other environmental regulatory processes (e.g. plant inputs and plant-mediated transport; [13,14,16]), but taken together, our results do indicate substantial potential variability in emissions of all three assessed GHGs across the peatlands in the basin.

## (c) Controls over greenhouse gas emissions

Correlation matrices revealed distinct GHG–environment relationships across hydrological regimes, underscoring dynamic environmental controls on biogeochemical cycling in tropical peatlands (figure 7). Moderate correlations between $N_2O$ and trace metals such as Zn and Cd in mesic conditions may reflect microbial pathways sensitive to micronutrient availability or redox fluctuations in transitional zones [42]. Weaker and more diffuse GHG correlations in flooded aerobic conditions are likely influenced by fluctuating oxygen levels and intermediate redox states that support diverse but less specialized microbial communities [43,44]. The flooded anoxic regime exhibited the strongest and most coherent patterns, with $CO_2$ showing consistently strong positive correlations with Ca, Mg and Mn, suggesting that anaerobic decomposition processes are tightly coupled with geochemical mobilization under reduced conditions [45]. These findings highlight the importance of hydrological context in shaping the interplay between GHG production and peat chemistry, indicating distinct regulatory mechanisms across redox gradients.

Strong correlations between several environmental variables and NMDS ordination axes suggest that S, Fe and P play a dominant role in structuring peat chemistry across vegetation types (figure 8). High $R^2$ values (e.g. S: 0.90; Fe: 0.73) are supported by robust permutation-based significance testing and a stress level of 0.066. In addition, the influence of these variables is ecologically plausible, given that S and Fe are key indicators of redox conditions and microbial activity in wetland soils [46,47], alongside the consistency of these strong associations with known biogeochemical processes, including $CH_4$ production [47,48]). Although the ordination was performed independently of GHG data to reduce the risk of circularity, the relatively tight clustering of samples in figure 8 suggests that some homogeneity within vegetation types may contribute to the strength of observed relationships (supplementary material, table S2).

The RF models, despite variable model performance, reveal distinct patterns for $CO_2$, $CH_4$ and $N_2O$ production/consumption across hydrological regimes (table 1). For instance, $CO_2$ production was more predictable under flooded aerobic conditions, suggesting stronger control by oxygen-sensitive processes such as root respiration and aerobic decomposition [5,49]. Vegetation was only identified as a top predictor of $CO_2$ production under mesic conditions, although it likely exerts an indirect effect on other variables (e.g. impacting nutrient availability, organic matter properties and/or rhizosphere pH). By contrast, $CH_4$ and $N_2O$ production/consumption potential was best predicted under mesic conditions. Variable importance rankings emphasized the influence of both substrate quality (e.g. total carbon and FTIR-derived lignin : carbohydrate ratio) and redox-sensitive elements (e.g. Fe, Zn and Mn), indicating a coupled role of carbon availability and biogeochemical constraints in regulating GHG emissions (figure 9).

Proximity to rivers also strongly influenced GHG dynamics, particularly for $CO_2$ and $N_2O$, highlighting the importance of spatial context in determining GHG dynamics across the basin. This suggests that river flood patterns are likely to be an important driver of *in situ* emissions. During periods of inundation, high emissions *in situ* can be directly linked to water levels, but the effect of flooding is likely longer lasting through the impacts of sediment inputs from seasonal river flooding, which may affect organic matter availability, and the presence of trace elements involved in the microbially mediated pathways of GHG production [50]. Supporting this, Cu, Al, Ni, Fe, Mo and Mn were all identified as correlates of $CH_4$ production through our analysis, and likely act through a combination of direct and indirect mechanisms: Ni is a metal co-factor for the enzyme methyl-coenzyme M reductase, which catalyses the final step in $CH_4$ production [51], while Mo is similarly an enzymatic co-factor using $CO_2$ reduction pathways by hydrogenotrophic methanogens [52]. The reduction of Fe(III) to Fe(II) is an important component of methanogenesis, acting as a terminal electron acceptor, while Mn is similarly important for redox reactions [46,53]. Cu is not directly involved in methanogenesis, but may support enzymes in methanotrophs in low concentrations, influencing the balance of $CH_4$ production and consumption, while at higher concentrations, it can be toxic for methanogens, thereby inhibiting $CH_4$ production [46]. Al has previously been demonstrated as negatively impacting $CH_4$ emissions [54], but little is known about its mechanistic role in driving GHG dynamics. Most likely, Al concentration has an indirect effect by impacting peat microbial community structure and function [55].

pH was also identified as playing an important role in GHG production under differing hydrological regimes, most likely owing to its direct impacts on microbial community structure and activity, enzyme function, redox processes and nutrient availability. Microbial communities responsible for GHG production and consumption (e.g. methanogens, methanotrophs, denitrifiers and nitrifiers) are highly sensitive to pH changes [14,15]. Very low pH values have previously been linked to low $CH_4$ and $CO_2$ production [56]. While peat in this study had a pH of 3.4–4 (supplementary material, table S1), the optimal pH for methanogenesis is higher (6–7) [57]. Low pH inhibits the final step of denitrification ($N_2O$ to $N_2$), leading to greater $N_2O$ release [38].

Together, our analyses reveal that GHG production/consumption potential and peat chemistry in tropical peatlands are governed by a combination of hydrological regime, substrate quality and biogeochemical context. Correlation matrices showed that GHG–environment relationships are highly regime-specific, with flooded anoxic conditions exhibiting the strongest and most coherent associations. The NMDS ordination further highlighted clear compositional differences in peat chemistry across vegetation types and sites, with vectors such as S, Fe and P explaining a large proportion of the variation in surface peat chemistry. RF models identified similar drivers as key predictors of GHG fluxes, although predictive performance varied by gas and hydrological context. Notably, $CO_2$ emissions were best predicted under flooded aerobic conditions, while $CH_4$ and $N_2O$ were better explained in mesic settings, suggesting differential microbial and physico-chemical controls. Across analyses, variables related to nutrient availability (P and K), redox status (Fe and S), and organic matter quality (TC and FTIR ratio) consistently emerged as key controls, reinforcing their central role in mediating both peat chemistry and GHG dynamics in tropical peatlands. These findings highlight the importance of considering hydrological variability and edaphic gradients when assessing the vulnerability of peatland GHG emissions to environmental change.

## (d) Implications for environmental change

Climate change and land use pressures are widely established to pose a significant threat to tropical peatland ecosystems, as well as the communities that rely on them [58–61], and can have substantial implications for the balance of GHG production [5,6]. Previous work in peatlands in the central Congo Basin indicates that drier conditions lead to rapid decomposition of peat [23,62]. Reduced rainfall, prolonged droughts or drainage for agriculture result in lower water levels, increasing oxygen penetration and stimulating aerobic decomposition, thereby elevating $CO_2$ emissions (figure 2). Conversely, extreme rainfall and flooding can create extended anoxic conditions, promoting $CH_4$ production while inhibiting $CH_4$ oxidation (figure 3).

The climatic vulnerabilities of tropical peatlands in the region are further compounded by increasing risks from land-use change. Conversion of peatlands to agriculture, for example, for oil palm cultivation as widely seen in Malaysia and Indonesia [63], would likely amplify GHG production and emissions in the Congo Basin. In Southeast Asia, large-scale drainage

for plantations has led to substantial $CO_2$ release, peat subsidence and elevated fire risk [17,61,64,65]. Similar outcomes are likely in Central Africa if drainage and vegetation conversion occur at scale. Shifting from natural palm- and hardwood- to palm oil-dominated systems may not only increase substrate availability for microbial decomposition, but also disrupt redox-sensitive nutrient cycles and microbial processes and alter inputs and organic matter turnover [9], further enhancing GHG fluxes (figure 9). Moreover, land conversion reduces vegetation diversity, limiting the ecological resilience of peatlands to climate extremes. Given the strong correlations between hydrological regime, trace element dynamics and GHG emissions observed in this study, maintaining intact, undrained peat swamp forests is crucial for mitigating future climate feedbacks and preserving the substantial carbon sink capacity of Central African peatlands [3,23]. Protection of tropical peatlands as intact hydrological units is fundamental to achieving this [66].

## 5. Conclusions

We have shown that the hydrological regime represents a key control over the production and emission of GHGs from peats from the central Congo Basin peatland complex, further moderated by the dominant vegetation type (palm versus peat-dominated peatlands) which exerted a significant impact on a range of peat chemical properties. The balance of production and consumption processes for all measured GHGs from the region broadly matches those measured in other equivalent incubation studies, but exhibited substantial spatial variability, highlighting the importance of local site characteristics in driving emissions. RF model performance and key predictors varied substantially by hydrological condition, further reinforcing the importance of regime-specific controls on GHG emissions in tropical peatlands. Across palm- and hardwood-dominated peatland sites, GHG production occurred predominantly in surface peats, declining with depth, matching trends in substrate availability indicated through Rock-Eval pyrolysis data. Taken together, our results underline the substantial spatial variation in GHG production and emissions from peatlands in the central Congo Basin, and underline the impact of hydrology and vegetation type in driving emissions, and thus their potential sensitivity to environmental change. Given the extensive peat deposits in the region and their global importance as a carbon store, processes that accelerate decomposition (e.g. changes in hydrology or climatic warming) are likely to substantially alter the balance of production and consumption, with implications for global environmental change.

Ethics. This work did not require ethical approval from a human subject or animal welfare committee.

Data accessibility. Data is available in electronic supplementary materials.

Supplementary material is available online [67].

Declaration of AI use. We have not used AI-assisted technologies in creating this article.

Authors' contributions. N.G.: conceptualization, data curation, formal analysis, funding acquisition, investigation, methodology, project administration, resources, validation, visualization, writing—original draft, writing—review and editing; A.J.: methodology, validation, visualization, writing—review and editing; H.C.: data curation, investigation, methodology; S.S.: data curation, funding acquisition, investigation, methodology, resources, supervision, writing—review and editing; A.J.J.-S.: methodology, writing—review and editing; Y.E.B.: investigation, methodology, writing—review and editing; P.B.: investigation, methodology, writing—review and editing; A.B.: funding acquisition, validation, writing—review and editing; H.C.: investigation, methodology, writing—review and editing; B.C.: investigation, methodology, writing—review and editing; D.E.C.: investigation, methodology, writing—review and editing; G.D.: investigation, methodology, writing—review and editing; O.E.B.: investigation, methodology, writing—review and editing; J.K.: investigation, methodology, writing—review and editing; I.L.: funding acquisition, investigation, methodology, writing—review and editing; Y.E.W.M.: investigation, methodology, writing—review and editing; M.M.: investigation, methodology, writing—review and editing; V.M.H.: investigation, methodology, writing—review and editing; G.R.M.N.: investigation, methodology, writing—review and editing; S.E.P.: investigation, methodology, writing—review and editing; K.R.: investigation, methodology, writing—review and editing; C.H.V.: funding acquisition, investigation, methodology, writing—review and editing; C.E.N.E.: funding acquisition, methodology, project administration, writing—review and editing; S.I.: funding acquisition, investigation, methodology, writing—review and editing; S.L.L.: funding acquisition, investigation.

All authors gave final approval for publication and agreed to be held accountable for the work performed therein.

Conflict of interest declaration. We declare we have no competing interests.

Funding. This work was supported by the Natural Environment Research Council (grant nos. NE/R016860/1 and NE/X015238/1) awarded to S.L.L., N.T.G., respectively. S.L.L. was further supported by a Greenpeace Fund Award. N.T.G. further acknowledges funding from the Royal Geographical Society and Royal Society (IES\R1\241246). Rock-Eval analyses were partially funded from project NEE4699S (Organic Geochemistry Facility, BGS).

Acknowledgements. We thank the communities that hosted and assisted with our fieldwork in the Republic of Congo (Bondzale, Ekolongouma and Itanga) and Democratic Republic of Congo (Mpeka, Bondamba, Bolengo and Boboka). We thank the Groupe d'action pour sauver l'homme et son environnement (GASHE), especially J. Mathe, Greenpeace Africa and R. Monsembula, and the Wildlife Conservation Society, especially B. Evans, for essential logistical support. We thank the governments of the Republic of Congo and Democratic Republic of the Congo, the Province of Équateur and the Ministry of Environment and Sustainable Development for assistance with our fieldwork. We thank B. Bongwemisa, J. Sando, J.P. Lokila, P. Bosange, F. Mongonga and R. Kendewa for essential field support; Helen Plante for support with project communications; the CongoPeat network provided invaluable discussions and feedback. We would also like to thank the handling editor, and two anonymous reviewers, whose feedback substantially improved the manuscript.

## References

1. Dargie GC, Lewis SL, Lawson IT, Mitchard ETA, Page SE, Bocko YE, Ifo SA. 2017 Age, extent and carbon storage of the central Congo Basin peatland complex. *Nature* **542**, 86–90. (doi:10.1038/nature21048)

2. Biddulph GE *et al.* 2021 Current knowledge on the Cuvette Centrale peatland complex and future research directions. *Bois For. Trop.* **350**, 3–14. (doi:10.19182/bft2021.350.a36288)
3. Crezee B *et al.* 2022 Mapping peat thickness and carbon stocks of the central Congo Basin using field data. *Nat. Geosci.* **15**, 639–644. (doi:10.1038/s41561-022-00966-7)
4. Georgio S *et al*. 2022 What determines peat swamp vegetation type in the Central Congo Basin? *EGUsphere*, 1–39. (doi:10.5194/egusphere-2022-580)
5. Girkin NT, Vane CH, Turner BL, Ostle NJ, Sjögersten S. 2020 Root oxygen mitigates methane fluxes in tropical peatlands. *Environ. Res. Lett.* **15**, 064013. (doi:10.1088/1748-9326/ab8495)
6. Sjögersten S, Aplin P, Gauci V, Peacock M, Siegenthaler A, Turner BL. 2018 Temperature response of ex-situ greenhouse gas emissions from tropical peatlands: interactions between forest type and peat moisture conditions. *Geoderma*. **324**, 47–55 (doi:10.1016/j.geoderma.2018.02.029)
7. Cooper H, Davidson S, Gauci V, Girkin N. 2024 Plant controls over tropical wetland nitrous oxide dynamics: a review. *Trop. Ecol.* **66**, 550–558. (doi:10.1007/s42965-025-00407-7)
8. Girkin NT, Cooper HV. 2022 Nitrogen and ammonia in soils. *Reference Module in Earth Systems and Environmental Sciences*. Elsevier [online] (doi:10.1016/B978-0-12-822974-3.00010-0)
9. Upton A, Vane CH, Girkin N, Turner BL, Sjögersten S. 2018 Does litter input determine carbon storage and peat organic chemistry in tropical peatlands? *Geoderma* **326**, 76–87. (doi:10.1016/j.geoderma.2018.03.030)
10. Girkin N, Vane C, Cooper H, Moss-Hayes V, Craigon J, Turner BL, Ostle N, Sjögersten S. 2019 Spatial variability of organic matter properties determines methane fluxes in a tropical forested peatland. *Biogeochemistry* **142**, 231–245. (doi:10.1007/s10533-018-0531-1)
11. Hoyos-Santillan J, Lomax BH, Large D, Turner BL, Boom A, Lopez OR, Sjögersten S. 2015 Getting to the root of the problem: litter decomposition and peat formation in lowland neotropical peatlands. *Biogeochemistry* **126**, 115–129. (doi:10.1007/s10533-015-0147-7)
12. Hoyos-Santillan J, Lomax BH, Large D, Turner BL, Boom A, Lopez OR, Sjogersten S. 2016 Quality not quantity: organic matter composition controls of CO2 and CH4 fluxes in neotropical peat profiles. *Soil Biol. Biochem.* **103**, 86–96. (doi:10.1016/j.soilbio.2016.08.017)
13. Pangala SR *et al.* 2017. Large emissions from floodplain trees close the Amazon methane budget. *Nature* **552**, 230–234. (doi:10.1038/nature24639)
14. Girkin NT, Turner BL, Ostle N, Craigon J, Sjögersten S. 2018 Root exudate analogues accelerate $CO_2$ and $CH_4$ production in tropical peat. *Soil Biol. Biochem.* **117**, 48–55. (doi:10.1016/j.soilbio.2017.11.008)
15. Girkin NT, Turner BL, Ostle N, Sjögersten S. 2018 Composition and concentration of root exudate analogues regulate greenhouse gas fluxes from tropical peat. *Soil Biol. Biochem.* **127**, 280–285. (doi:10.1016/j.soilbio.2018.09.033)
16. Raza S, Cooper HV, Girkin NT, Kent MS, Bennett MJ, Mooney SJ, Colombi T. 2025 Missing the input: the underrepresentation of plant physiology in global soil carbon research. *SOIL* **11**, 363–369. (doi:10.5194/soil-11-363-2025)
17. Cooper HV, Evers S, Aplin P, Crout N, Dahalan MPB, Sjögersten S. 2020 Greenhouse gas emissions resulting from conversion of peat swamp forest to oil palm plantation. *Nat. Commun.* **11**, 407. (doi:10.1038/s41467-020-14298-w)
18. Hawthorne D *et al.* 2023 Genesis and development of an interfluvial peatland in the central Congo Basin since the late Pleistocene. *Quat. Sci. Rev.* **305**, 107992. (doi:10.1016/j.quascirev.2023.107992)
19. Samba G, Nganga D, Mpounzam M. 2008 Rainfall and temperature variations over Congo-Brazzaville between 1950 and 1998. *Theor. Appl. Climatol*. **91**, 85–97, (doi:10.1007/s00704-007-0298-0)
20. Brown C, Boyd DS, Sjögersten S, Vane CH. 2023 Detecting tropical peatland degradation: combining remote sensing and organic geochemistry. *PLoS ONE* **18**, e0280187. (doi:10.1371/journal.pone.0280187)
21. Cooper HV, Vane CH, Evers S, Aplin P, Girkin NT, Sjögersten S. 2019 From peat swamp forest to oil palm plantations: the stability of tropical peatland carbon. *Geoderma* **342**, 109–117. (doi:10.1016/j.geoderma.2019.02.021)
22. Newell AJ, Vane CH, Sorensen JPR, Moss-Hayes V, Gooddy DC. 2016 Long-term Holocene groundwater fluctuations in a chalk catchment: evidence from Rock-Eval pyrolysis of riparian peats. *Hydrol. Process.* **30**, 4556–4567 (doi:10.1002/hyp.10903)
23. Garcin Y *et al.* 2022 Hydroclimatic vulnerability of peat carbon in the central Congo Basin. *Nature* **612**, 277–282. (doi:10.1038/s41586-022-05389-3)
24. Girkin NT, Santos RL, dos Vane CH, Ostle N, Turner BL, Sjögersten S. 2020 Peat properties, dominant vegetation type and microbial community structure in a tropical peatland. *Wetlands* **40**, 1367–1377 (doi:10.1007/s13157-020-01287-4)
25. Sebag D *et al.* 2016 Dynamics of soil organic matter based on new Rock-Eval indices. *Geoderma* **284**, 185–203. (doi:10.1016/j.geoderma.2016.08.025)
26. Tonks AJ, Aplin P, Beriro DJ, Cooper H, Evers S, Vane CH, Sjögersten S. 2017 Impacts of conversion of tropical peat swamp forest to oil palm plantation on peat organic chemistry, physical properties and carbon stocks. *Geoderma* **289**, 36–45. (doi:10.1016/j.geoderma.2016.11.018)
27. Kačuráková M, Wilson RH. 2001 Developments in mid-infrared FT-IR spectroscopy of selected carbohydrates. *Carbohydr. Polym.* **44**, 291–303.
28. R Core Team. 2021 *R: A language and environment for statistical computing*. https://www.R-project.org/.
29. Oksanen J *et al.* 2022 Vegan: community ecology package. R package v. 2. See https://CRAN.R-project.org/package=vegan.
30. Teh YA, Murphy WA, Berrio JC, Boom A, Page SE. 2017 Seasonal variability in methane and nitrous oxide fluxes from tropical peatlands in the western Amazon basin. *Biogeosciences* **14**, 3669–3683. (doi:10.5194/bg-14-3669-2017)
31. Zeikus JG. 1981 Lignin metabolism and the carbon-cycle—polymer biosynthesis, biodegradation, and environmental recalcitrance. *Adv. Microb. Ecol.* **5**, 211–243.
32. Hoyos-Santillan J, Lomax BH, Large D, Turner BL, Boom A, Lopez OR, Sjögersten S. 2015 Getting to the root of the problem: litter decomposition and peat formation in lowland Neotropical peatlands. *Biogeochemistry* **126**, 115–129. (doi:10.1007/s10533-015-0147-7)
33. Ek M, Gellerstedt G, Henriksson G (eds). 2009 *Wood chemistry and wood biotechnology*, vol. 1. Berlin, Germany: Walter de Gruyter.
34. Vane CH, Kim AW, Moss-Hayes V, Snape CE, Castro-Diaz M, Khan NS, Engelhart SE, Horton BP. 2013 Mangrove tissue decay by arboreal termites (*Nasutitermes acajutlae*) and their role in the mangrove C cycle (Puerto Rico): chemical characterisation and organic matter provenance using bulk δ13C, C/N, alkaline CuO oxidation-GC/MS and solid-state 13C NMR. *Geochem. Geophys. Geosyst.* **14**, 3176–3191. (doi:10.1002/ggge.20194)
35. Girkin NT, Turner BL, Ostle N, Craigon J, Sjögersten S. 2018 Root exudate analogues accelerate $CO_2$ and $CH_4$ production in tropical peat. *Soil Biol. Biochem.* **117**, 48–55. (doi:10.1016/j.soilbio.2017.11.008)
36. Wright EL, Black CR, Cheesman AW, Drage T, Large D, Turner BL, Sjögersten S. 2011 Contribution of subsurface peat to CO2 and CH4 fluxes in a neotropical peatland. *Global Change Biol.* **17**, 2867–2881. (doi:10.1111/j.1365-2486.2011.02448.x)
37. Girkin NT, Dhandapani S, Evers S, Ostle N, Turner BL, Sjögersten S. 2020 Interactions between labile carbon, temperature and land use regulate carbon dioxide and methane production in tropical peat. *Biogeochemistry* **147**, 87–97. (doi:10.1007/s10533-019-00632-y)

38. Girkin NT, Siegenthaler A, Lopez O, Stott A, Ostle N, Gauci V, Sjögersten S. 2025 Plant root carbon inputs drive methane production in tropical peatlands. *Sci. Rep.* **15**, 3244. (doi:10.1038/s41598-025-87467-w)
39. Reddy KR, Patrick WH, Lindau CW. 1989 Nitrification–denitrification at the plant root–sediment interface in wetlands. *Limnol. Oceanogr.* **34**, 1004–1013. (doi:10.4319/lo.1989.34.6.1004)
40. Jovani-Sancho AJ *et al.* 2023 $CH_4$ and $N_2O$ emissions from smallholder agricultural systems on tropical peatlands in Southeast Asia. *Global Change Biol.* **29**, 4279–4297. (doi:10.1111/gcb.1674)
41. Bateman EJ, Baggs EM. 2005 Contributions of nitrification and denitrification to $N_2O$ emissions from soils at different water-filled pore space. *Biol. Fertil. Soils.* **41**, 379–388. (doi:10.1007/s00374-005-0858-3)
42. Buessecker S *et al.* 2022 Coupled abiotic–biotic cycling of nitrous oxide in tropical peatlands. *Nat. Ecol. Evol.* **6**, 1881–1890. (doi:10.1038/s41559-022-01892-y)
43. Buessecker S, Zamora Z, Sarno AF, Finn DR, Hoyt AM, van Haren J, Cadillo-Quiroz H, Urquiza-Muñoz JD. 2021 Microbial communities and interactions of nitrogen oxides with methanogenesis in diverse peatlands of the Amazon basin. *Front. Microbiol.* **12**, 659079. (doi:10.3389/fmicb.2021.659079)
44. Finn DR, Ziv-El M, Van Haren J, Park JG, Aguila-Pasquel J, Urquiza-Muñoz JD, Cadillo-Quiroz H. 2020 Methanogens and methanotrophs show nutrient-dependent community assemblage patterns across tropical peatlands of the Pastaza-Marañón Basin, Peruvian Amazonia. *Front. Microbiol.* **11**, 746. (doi:10.3389/fmicb.2020.00746)
45. Stendahl J, Berg B, Lindahl BD. 2017 Manganese availability is negatively associated with carbon storage in northern coniferous forest humus layers. *Sci. Rep.* **7**, 15487. (doi:10.1038/s41598-017-15801-y)
46. Basiliko N, Yavitt JB. 2001 Influence of Ni, Co, Fe, and Na additions on methane production in *Sphagnum*-dominated Northern American peatlands. *Biogeochemistry* **52**, 133–153. (doi:10.1023/A:1006461803585)
47. Le Mer J, Roger P. 2001 Production, oxidation, emission and consumption of methane by soils: a review. *Eur. J. Soil Biol.* **37**, 25–50. (doi:10.1016/S1164-5563(01)01067-6)
48. Wright EL, Black CR, Turner BL, Sjögersten S. 2013 Environmental controls of temporal and spatial variability in $CO_2$ and $CH_4$ fluxes in a neotropical peatland. *Global Change Biol.* **19**, 3775–3789. (doi:10.1111/gcb.12330)
49. Girkin NT, Turner BL, Ostle N, Sjögersten S. 2018 Root-derived $CO_2$ flux from a tropical peatland. *Wetlands Ecol. Manage.* **26**, 985–991. (doi:10.1007/s11273-018-9617-8)
50. Wang S, Wu S, Dong Y, Li X, Wang Y, Li Y, Zhu Y, Deng J, Zhuang X. 2024 River-lake ecosystems exhibit a strong seasonal cycle of greenhouse gas emissions. *Commun. Earth Environ.* **5**, 784. (doi:10.1038/s43247-024-01912-8)
51. Spietz RL, Payne D, Boyd ES. 2023 Methanogens acquire and bioaccumulate nickel during reductive dissolution of nickelian pyrite. *Appl. Environ. Microbiol.* **89**, e00991-23. (doi:10.1128/aem.00991-23)
52. Mares S, Moreno-Andrade I, Quijano G. 2023 Biological $CH_4$ production from $H_2/CO_2$ streams: influence of trace metals concentration on the hydrogenotrophic process. *J. Environ. Chem. Eng.* **11**, 109528. (doi:10.1016/j.jece.2023.109528)
53. Min SF, Chang Z, Chen L, Feng LZ, Tang B, Ping ZZ. 2019 Effects of manganese pollution on soil microbial community function and plant growth. *J. Environ. Protect. Ecol.* **20**, 64–73.
54. Dhandapani S, Girkin NT, Evers S, Ritz K, Sjögersten S. 2020 Is intercropping an environmentally-wise alternative to established oil palm monoculture in tropical peatlands? *Front. For. Global Change* **3**, 70. (doi:10.3389/ffgc.2020.00070)
55. Dhandapani S, Evers S, Ritz K, Sjögersten S. 2021 Nutrient and trace element concentrations influence greenhouse gas emissions from Malaysian tropical peatlands. *Soil Use Manag.* **37**, 138–150. (doi:10.1111/sum.12669)
56. Ye R, Jin Q, Bohannan B, Keller JK, McAllister SA, Bridgham SD. 2012 pH controls over anaerobic carbon mineralization, the efficiency of methane production, and methanogenic pathways in peatlands across an ombrotrophic–minerotrophic gradient. *Soil Biol. Biochem.* **54**, 36–47. (doi:10.1016/j.soilbio.2012.05.015)
57. Dunfield P, Knowles R, Dumont R, Moore TR. 1993 Methane production and consumption in temperate and sub-arctic peat soils—response to temperature and ph. *Soil Biol. Biochem.* **25**, 321–326. (doi:10.1016/0038-0717(93)90130-4)
58. Cole LES *et al.* 2022 Tropical peatlands in the anthropocene: lessons from the past. *Anthropocene* **37**, 100324. (doi:10.1016/j.ancene.2022.100324)
59. Girkin N *et al.* 2023 The three-peat challenge: business as usual, responsible agriculture, and conservation and restoration as management trajectories in global peatlands. *Carbon Manage.* **14**, 2275578. (doi:10.1080/17583004.2023.2275578)
60. Loisel J *et al*. 2021 Expert assessment of future vulnerability of the global peatland carbon sink. *Nat. Clim. Change* **11**, 70–77. (doi:10.1038/s41558-020-00944-0)
61. Girkin NT *et al.* 2022 Tropical peatlands in the Anthropocene: the present and the future. *Anthropocene* **40**, 100354. (doi:10.1016/j.ancene.2022.100354)
62. Young DM *et al.* 2023 Simulating carbon accumulation and loss in the central Congo peatlands. *Global Change Biol.* **29**, 6812–6827. (doi:10.1111/gcb.16966)
63. Miettinen J, Hooijer A, Tollenaar D, Page S, Malins C, Vernimmen R, Liew SC, Shi C. 2012 *Historical analysis and projection of oil palm plantation expansion on peatland in Southeast Asia*. International Council for Clean Transport White Paper 17. See https://theicct.org/wp-content/uploads/2021/06/ICCT_palm-expansion_Feb2012.pdf.
64. Page SE, Siegert F, Rieley JO, Boehm HDV, Jaya A, Limin S. 2002 The amount of carbon released from peat and forest fires in Indonesia during 1997. *Nature* **420**, 61–65. (doi:10.1038/nature01131)
65. Page SE, Baird AJ. 2016 Peatlands and global change: response and resilience. *Ann. Rev. Environ. Res.* **41**, 35–57. (doi:10.1146/annurev-environ-110615-085520)
66. Girkin NT, Davidson SJ. 2024 Protect peatlands to achieve climate goals. *Science* **383**, 490. (doi:10.1126/science.adn4001)
67. Girkin N *et al*. 2026 Supplementary material from: Environmental controls over greenhouse gas dynamics of tropical peatlands of the Central Congo Basin. Figshare. (doi:10.6084/m9.figshare.c.8566722)